

MIT Open Access Articles

Nanoengineered Surfaces for Efficient Energy Systems

The MIT Faculty has made this article openly available. **Please share** how this access benefits you. Your story matters.

Citation: Wang, Evelyn N., Rong Xiao, Kuang-Han Chu, and Ryan Enright. "Nanoengineered Surfaces for Efficient Energy Systems." ASME 2011 9th International Conference on Nanochannels, Microchannels, and Minichannels, Volume 2, 19-22 June, 2011, Edmonton, Alberta, Canada, ASME, 2011. © 2011 ASME

As Published: <http://dx.doi.org/10.1115/ICNMM2011-58300>

Publisher: ASME International

Persistent URL: <http://hdl.handle.net/1721.1/120176>

Version: Final published version: final published article, as it appeared in a journal, conference proceedings, or other formally published context

Terms of Use: Article is made available in accordance with the publisher's policy and may be subject to US copyright law. Please refer to the publisher's site for terms of use.



ICNMM2011-58' \$\$

NANOENGINEERED SURFACES FOR EFFICIENT ENERGY SYSTEMS

Evelyn N. Wang, Rong Xiao, Kuang-Han Chu, and Ryan Enright
Device Research Laboratory, Department of Mechanical Engineering, MIT
Cambridge, MA, USA

ABSTRACT

Nanoengineered surfaces offer new possibilities to manipulate fluid transport and enhance heat dissipation characteristics for the development of efficient energy systems. In particular, nanostructures on these surfaces can be harnessed to achieve superhydrophilicity and superhydrophobicity, and to control liquid behavior and phase-change processes. In this work, we will describe recent developments focused on using superhydrophilic nanostructure design to manipulate liquid spreading behavior and directionalities. In the presence of asymmetric nanopillars, uni-directional spreading of water droplets can be achieved where the liquid spreads only in the direction of the pillar deflection and becomes pinned on the opposite interface. In the presence of fine features on the pillars, we observed a multi-layer spreading effect due to their associated energy barriers. For both cases, we have developed energy-based models to accurately predict the liquid behavior as functions of pertinent parameters. Furthermore, we developed a semi-analytical model to predict liquid propagation rates in pillar arrays driven by capillarity. The results offer design guidelines to optimize propagation rates for fluidic wicks. These investigations offer insights and significant potential for the development and integration of advanced nanostructures to achieve efficient energy conversion systems.

INTRODUCTION

A significant body of research in the past few decades have focused on using nanoengineered surfaces to achieve extreme static contact angles by magnifying the intrinsic hydrophobicity or hydrophilicity (1-5). More recently, such surfaces have received interest to control and enhance fluid and heat transport processes to develop efficient energy systems. Specifically, a significant bottleneck in renewable energy systems is related to the thermal management demands that limit energy conversion efficiencies. For example, in concentrated photovoltaic systems

(PVs), the inefficiencies in the cells result in significant heat generation that decreases electrical power output (6, 7) and leads to long-term degradation in the cells (8). Solar thermoelectrics (9), solar thermophotovoltaics (10), and conventional solar thermal systems (11) face similar challenges where compact and efficient cooling solutions are needed to effectively transport and dissipate heat generated from these systems. The incorporation of nanostructure design using fluidic based cooling promise the development of passive, compact, and high heat flux solutions (12, 13). However, the rich physics associated with the complex fluid and heat interactions with nanostructures need to be well understood before taking advantage of surface design.

This paper summarizes recent developments using superhydrophilic three-dimensional nanostructure design to manipulate fluid behavior. We demonstrated that uni-directional and multi-layer spreading can be achieved. We developed energy-based models to accurately predict the liquid behavior as functions of pertinent parameters. In addition, we also present a model that offers design guidelines for the optimization of propagation rates in structured arrays driven by capillarity. These fundamental studies serve as a first step towards incorporating nanostructures for high performance thermal strategies to achieve efficient energy conversion systems.

NANOSTRUCTURE FABRICATION

We designed and fabricated three-dimensional hydrophilic nanostructured surfaces to investigate the effect of geometry on liquid behavior. The structures were fabricated in silicon, where the pillar diameters ranged from 200 nm - 5 μm with heights from 5-10 μm . The pillars were defined using projection or contact lithography, and etched using deep reactive ion etching (DRIE). During the DRIE process, the etch and passivation cycles were varied to create intentional side scallops on the nanopillars, as shown in Fig. 1a. In addition, asymmetric

nanostructures were fabricated, by subsequently depositing a thin film of gold on one side of the pillars, as shown in Fig. 1b. The thickness of the gold film determined the deflection angle, owing to the residual stresses between the two materials. The surfaces were then conformally coated with a hydrophilic polymer (where the contact angle of water on a polymer coated flat surface is 80°) to achieve uniform surface properties. The deflection angles ranged from 0-52 degrees.

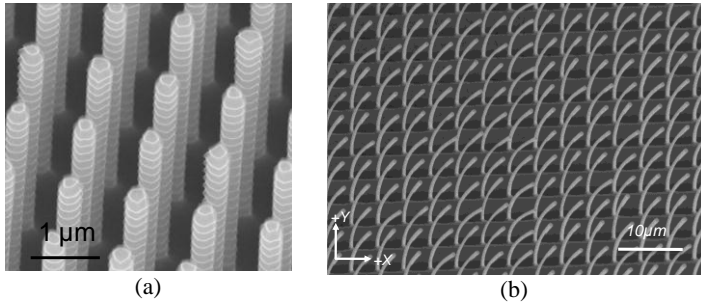


Fig 1. Three-dimensional nanostructures fabricated in silicon. a) Nanopillars with side scallops on the sides of the features. b) Asymmetric nanostructures deflected at approximately 12 degrees.

Detailed studies of liquid behavior on the nanostructures were carried out. Deionized water (DI) with varying concentrations of surfactant (Triton X-100) ranging from 0.01% to 0.00125% by volume was used to vary the surface tension from 30.2 to 42.6 dynes/cm. Characterization techniques include environmental scanning electron microscopy, fluorescence, white light, and interference microscopy, and high speed imaging.

UNI-DIRECTIONAL SPREADING

We investigated the effect asymmetric nanostructure design on liquid behavior (Fig. 1b) (14). Typical uni-directional spreading behavior on the fabricated asymmetric nanostructures is shown in the time-lapse images in Fig. 2. In this particular case, deionized (DI) water with a 0.002% concentration of surfactant (Triton X-100) by volume was deposited on the surface where the nanopillar deflection angle is 12° . The liquid propagates primarily towards the right, while the contact line pins in both the left and perpendicular directions (into the page).

We determined that the behavior of the liquid film was well-correlated with the behavior of the macroscopic droplet, *i.e.*, the liquid film propagation determines the direction of the macroscopic droplet spreading. To explain the uni-directional liquid film propagation, we developed a simple two-dimensional geometric model where the pillars were simplified as slanted rectangles in the 2D model, detailed in (14). The model assumes that the liquid film propagate only if the contact line is able to reach the next row of pillars. In addition, when the liquid film propagates, the local contact angle of the liquid cannot be smaller than θ_{eq} according to Young's Equation [5]

due to the fact that θ_{eq} is the lowest energy state. Therefore, θ_{eq} of the liquid must be equal to or smaller than a critical angle defined as θ_{cr} , which is based on the pillar geometry.

To study the spreading behavior and validate the theoretical model, a series of experiments were conducted. We used DI water and DI water with surfactants (Triton X-100 with concentrations ranging from 0.01% to 0.00125% by volume) on the polymer (*poly(cyclohexyl methacrylate-co-divinyl benzene)*) coated surface with an equilibrium contact angle of 80° (DI water).

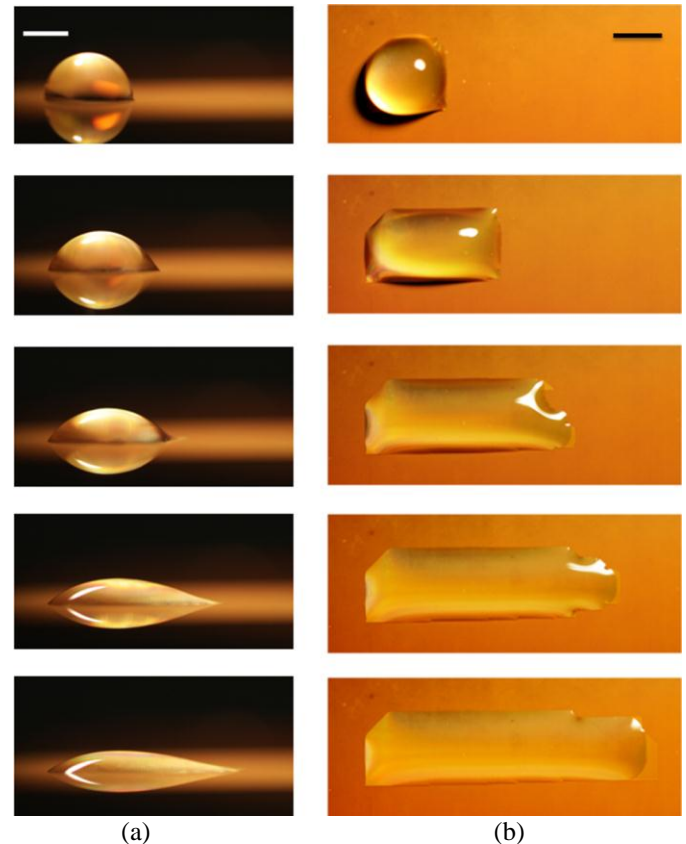


Fig. 2. Time-lapse images of uni-directional spreading of a liquid droplet. a) Side view and b) top view of a 1 μ L droplet of DI water with 0.002% by volume of surfactant spreading on a surface with pillar diameters of 500-750 nm, spacings of 3.5 μ m, and heights of 10 μ m deflected at 12° shown in Fig. 2. The contact line (left) stays pinned throughout the spreading process. The liquid film propagates in front of the macroscopic droplet. The scale bars are 1 mm.

Fig. 3 shows the experimental results of uni-directional spreading and the theoretical curves based on the geometric model. The model is plotted for the case $\theta_{cr} = \theta_{eq}$ in both +X (right) and -X (left) where the H/l (height-to-distance between pillars) ratio is 2.87 ($H = 10 \mu\text{m}$) for different pillar deflection angles and equilibrium contact angles. The region bound by

$\theta_{cr,-x}$ and $\theta_{eq} = 65^\circ$ (i.e., the imbibition condition) indicates the parameter space (in blue) that allows uni-directional spreading. The square symbols (\square) indicate experiments in which the liquid film propagates only in the +X direction, whereas the circles (\circ) are experiments where the film propagates directionally (in +X and -X). The triangles (Δ) show instances where the spreading is nearly uni-directional, i.e., the film propagates in -X but the propagation rate was at least five times slower than in +X. The crosses (\times) represent experiments where the film does not propagate at all due to the imbibition condition. The excellent agreement between the experimental results and theory suggest the ability to predict uni-directional spreading behavior using asymmetric nanostructure design. Such behavior can be harnessed to achieve fine control of liquid directionalities.

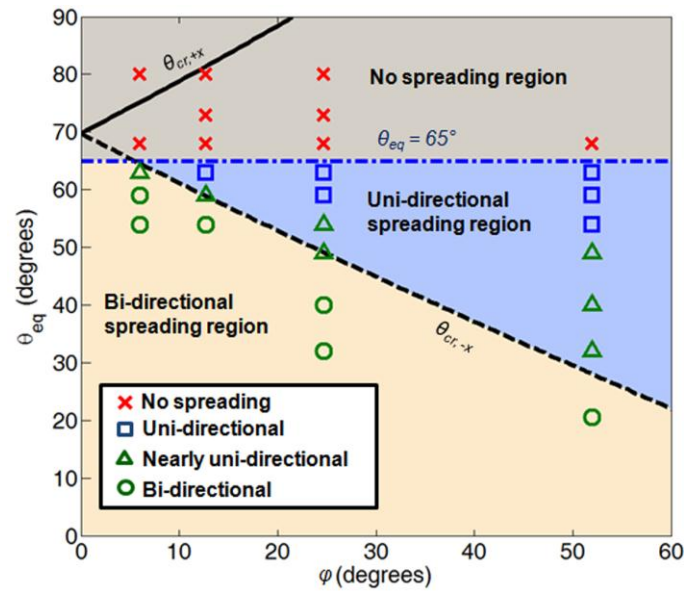


Fig. 3. Experimental results and the theoretical curves predicting uni-directional liquid spreading. The squares (\square), circles (\circ), triangles (Δ), and crosses (\times) show experimental results of uni-directional, bi-directional, nearly uni-directional, and no liquid propagation, respectively. The theoretical curves based on the proposed model are shown for $\theta_{eq} = \theta_{cr}$ with varying deflection angles, ϕ , for $H/l = 2.87$. The center region (blue) bound by $\theta_{cr,-x}$ and $\theta_{eq} = 65^\circ$ represents the parameter space that leads to uni-directional liquid spreading.

MULTI-LAYER SPREADING

For nanostructures, as shown in the scanning electron micrograph (SEM) in Fig. 1a, we observed liquid separation into multiple layers during the propagation across surfaces (15). A lower layer advances first, and subsequent sequential layers follows on top of the first one. The phenomenon shown in Fig. 4 was visualized with fluorescent microscopy with a 40 \times magnification (NA=0.60). A 29 mM Rhodamine B solution

was used to enhance the contrast between the visualized layers. The multi-layer separation was positively correlated to the presence of the scalloped features on the pillars, which creates energy barriers. When pillar arrays with the same diameter and spacing were fabricated but with non-visible scalloped features, the liquid spread across the surface with a uniform thickness.

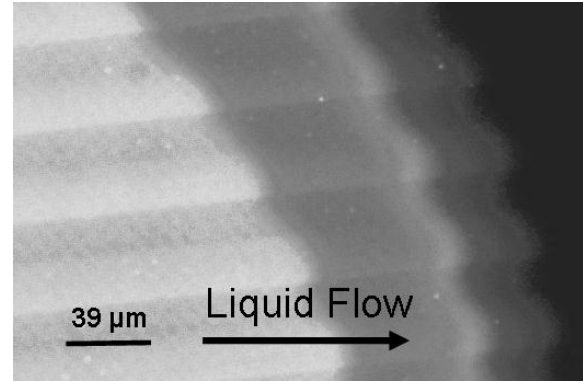


Fig. 4. Fluorescent image showing that the liquid is separated into multiple layers during spreading on the pillars shown in Fig.1a (15).

Therefore, we developed a model based on surface energy to explain the observations, which is detailed in (15). We simplified the scallops to tiered steps with an upper and lower height, h_u and h_l , upper and lower diameter, d_u , and d_l , respectively, where the distance between the centers of neighboring pillars is l . We also fabricated designs of the nanostructures with a single notch (to emulate a single scallop) with a defined size d_u , and height h_l to validate the theory.

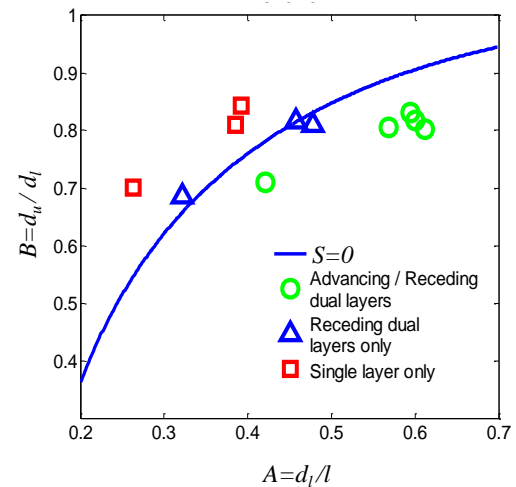


Fig. 5 Parameter space that determines the presence of single or dual layers for the case $C=h_l/(h_u+h_l)=0.49$.

Fig. 5 shows the results from the model compared with experiments for the case where the single notch is located at $C=$

$h_l/(h_u+h_l)=0.49$. The analytical curve in blue separates the regimes between single-layer and dual-layer spreading in the parameter space of $A=d/l$, and $B=d_u/d_l$. The experimental results show that the theoretical curve well demarcates the boundaries between geometries that lead to separated layers, and those that lead to a single layer, for both the advancing and receding processes. The results suggest that the spreading behavior can be controlled by choosing proper pillar geometries, which offer possibilities to control the thickness of liquid films on textured surfaces.

PREDICTION OF PROPAGATION RATES

In addition to predicting liquid behavior, quantitative understanding of liquid dynamics is needed. We investigated the simple case of uniformly spaced pillar arrays with liquid driven by capillarity. Washburn first proposed a model to predict liquid propagation rates in capillary tubes that balances capillary pressure with viscous resistance (16). Following Washburn's approach, we developed a semi-analytical model to predict liquid propagation rates based on the diameter, height, and period of the pillar arrays (17).

We determined the capillary pressure in the micropillar array using a thermodynamic approach minimizing interfacial free energy. The pressure is defined as the change in surface energy per unit volume, $P_{cap} = \Delta E / \Delta V$, where ΔE is the decrease in surface energy as the liquid fills one unit cell and ΔV is the corresponding volume of the liquid filling one unit cell. To accurately predict the change in surface energy and volume, Surface Evolver (SE) (18) was used to simulate the shape of the meniscus with minimum surface energy. Meanwhile, we validated the meniscus shape with interference microscopy. To determine the viscous resistance, we used the one-dimensional form of Brinkman's equation (19). By combining the proposed capillary pressure and viscous resistance models, an overall model to predict the propagation distance as a function of time is obtained, $x = Gt^{1/2}$ where P_{cap} is the capillary pressure determined and $G = (2P_{cap}/K)^{1/2}$ is defined as the propagation coefficient. Experiments were also performed on various microfabricated silicon pillars which show excellent agreement with the developed model.

We subsequently determined an effective propagation coefficient, $\mu G/\gamma$, that is functionally dependent on only the dimensionless geometrical parameters h/d and d/l , where μ is the viscosity of the liquid, G is the propagation coefficient, and γ is the surface tension. Fig. 6a shows the relationship for water on silicon pillars with various d/l and h/d ratios. The relationship is valid with $h \geq l$ and $d/l < 0.57$. The effective propagation coefficient can be interpreted as a competition between the viscous resistance and the driving capillary pressure. As the ratio of h/d increases, the effective propagation coefficient increases and approaches an upper theoretical limit as $h \rightarrow \infty$. When the ratio of d/l increases, the viscous resistance and the capillary pressure both increase and a maximum effective propagation coefficient is reached. Beyond this limit, the viscous resistance increases faster than the capillary

pressure, leading to a decrease in the effective propagation coefficient. The optimal d/l ratio and the corresponding maximum effective propagation coefficient for varying h/d ratios are shown in Fig. 6b. These results offer design guidelines to optimize micropillar geometries to enhance liquid transport.

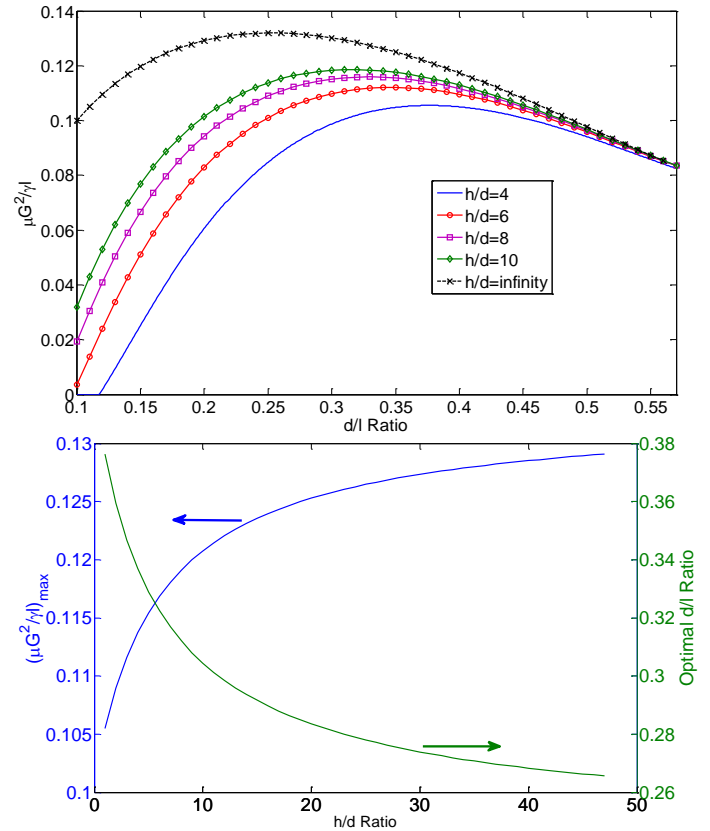


Fig. 6 Design guidelines for the optimization of pillar array geometries for $h \geq l$ and $d/l \leq 0.57$ (17). (a) Effective propagation coefficients predicted by the model for varying d/l and h/d ratios. (b) Design guidelines for maximum effective propagation coefficients on micropillar arrays with various aspect ratios and the corresponding optimal d/l ratios.

CONCLUSIONS

The work demonstrates that three-dimensional nanostructured surfaces offer new opportunities to achieve complex fluid behavior. We used a combination of experiments and modeling to explain the effect of nanopillar geometry and liquid surface tension on uni-directional and multi-layer spreading behavior. In addition, we developed a model to predict and optimize liquid propagation rates in pillar arrays. These fundamental studies promise exciting new possibilities to achieve new manipulation capability for compact and passive thermal management solutions to achieve efficient energy conversion systems.

ACKNOWLEDGMENTS

The authors gratefully acknowledge funding support from the National Science Foundation (under Award EEC-0824328), the DARPA Young Faculty Award, Office of Naval Research with Dr. Marc Spector as program manager, the Northrop Grumman New Faculty Innovation Grant, and the Intel Higher Education Grant. The authors would also like to acknowledge the M.I.T. Microsystems Technology Lab for fabrication staff support, help, and use of equipment, Baris Erinc Polat from Prof. Blankschtein's group and Salmaan Baxamusa and Mahriah Alf from Prof. Gleason's group in the Department of Chemical Engineering, M.I.T., for help with surface tension measurements and iCVD polymer deposition.

REFERENCES

1. Wenzel, R.N., *Resistance of Solid Surfaces to Wetting by Water*. Ind. Eng. Chem., 1936. **28**(8): p. 988-994.
2. Cassie, A.B.D. and S. Baxter, *Wettability of Porous Surfaces*. Trans. Faraday Soc., 1944. **40**: p. 546-551.
3. Quere, D., *Rough Ideas on Wetting*. Physica A-Statistical Mechanics And Its Applications, 2002. **313**(1-2): p. 32-46.
4. Patankar, N.A., *On the Modeling of Hydrophobic Contact Angles on Rough Surfaces*. Langmuir, 2003. **19**(4): p. 1249-1253.
5. Martinez, E., K. Seunarine, H. Morgan, N. Gadegaard, C.D.W. Wilkinson, and M.O. Riehle, *Superhydrophobicity and Superhydrophilicity of Regular Nanopatterns*. Nano Letters, 2005. **5**(10): p. 2097-2103.
6. Meneses-Rodríguez, P.P., J.G.-H. Horley, and Y.V. Vorobiev, *Photovoltaic Solar Cells Performance at Elevated Temperatures*. Solar Energy, 2005. **78**(2): p. 243-250.
7. Skoplaki, E. and J.A. Palyvos, *On the Temperature Dependence of Photovoltaic Module Electrical Performance: A Review of Efficiency/Power Correlations*. Solar Energy, 2009. **83**(5): p. 614-624.
8. Royne, A., C.J. Dey, and D.R. Mills, *Cooling of Photovoltaic Cells under Concentrated Illumination: A Critical Review*. Solar Energy Materials And Solar Cells, 2005. **86**(4): p. 451-483.
9. Lertsatitthanakorn, C., A. Therdyothin, and S. Soponronnarit, *Performance Analyses and Economic Evaluation of a Hybrid Thermoelectric Solar Water Heater*. Proceedings of the Institution of Mechanical Engineers Part a-Journal of Power and Energy, 2010. **224**(A5): p. 621-627.
10. Davies, P.A. and A. Luque, *Solar Thermophotovoltaics - Brief Review and a New Look*. Solar Energy Materials and Solar Cells, 1994. **33**(1): p. 11-22.
11. Mills, D., *Advances in Solar Thermal Electricity Technology*. Solar Energy, 2004. **76**(1-3): p. 19-31.
12. Nam, Y., S. Sharratt, C. Byon, S.J. Kim, and Y.S. Ju, *Fabrication and Characterization of the Capillary Performance of Superhydrophilic Cu Micropost Arrays*. Microelectromechanical Systems, Journal of, 2010. **19**(3): p. 581.
13. Srivastava, N., C.S. Din, A. Judson, N.C. MacDonald, and C.D. Meinhardt, *A Unified Scaling Model for Flow through a Lattice of Microfabricated Posts*. Lab On A Chip. **10**(9): p. 1148-1152.
14. Chu, K.H., R. Xiao, and E.N. Wang, *Uni-Directional Spreading on Asymmetric Nanostructured Surfaces*. Nature Materials, 2010. **9**: p. 413-417.
15. Xiao, R., K.H. Chu, and E.N. Wang, *Multilayer Liquid Spreading on Superhydrophilic Nanostructured Surfaces*. Applied Physics Letters, 2009. **94**(19).
16. Washburn, E.W., *The Dynamics of Capillary Flow*. Physical Review, 1921. **17**(3): p. 273.
17. Xiao, R., R. Enright, and E.N. Wang, *Prediction and Optimization of Liquid Propagation in Micropillar Arrays*. Langmuir, 2010. **26**(19): p. 15070-15075.
18. Brakke, K.A., *The Surface Evolver*. Experimental Mathematics, 1992. **1**(2): p. 141-165.
19. Brinkman, H., *A Calculation of the Viscous Force Exerted by a Flowing Fluid on a Dense Swarm of Particles*. Applied Scientific Research, 1949. **1**(1): p. 27.